LETTER

doi:10.1038/nature11611

Active upper–atmosphere chemistry and dynamics from polar circulation reversal on Titan

Nicholas A. Teanby[1], Patrick G. J. Irwin[2], Conor A. Nixon[3], Remco de Kok[4], Sandrine Vinatier[5], Athena Coustenis[5], Elliot Sefton-Nash[1,6], Simon B. Calcutt[2] & F. Michael Flasar[3]

Saturn's moon Titan has a nitrogen atmosphere comparable to Earth's, with a surface pressure of 1.4 bar. Numerical models reproduce the tropospheric conditions very well but have trouble explaining the observed middle-atmosphere temperatures, composition and winds[1,2]. The top of the middle-atmosphere circulation has been thought to lie at an altitude of 450 to 500 kilometres, where there is a layer of haze that appears to be separated from the main haze deck[3]. This 'detached' haze was previously explained as being due to the co-location of peak haze production and the limit of dynamical transport by the circulation's upper branch[4]. Here we report a build-up of trace gases over the south pole approximately two years after observing the 2009 post-equinox circulation reversal, from which we conclude that middle-atmosphere circulation must extend to an altitude of at least 600 kilometres. The primary drivers of this circulation are summer-hemisphere heating of haze by absorption of solar radiation and winter-hemisphere cooling due to infrared emission by haze and trace gases[5]; our results therefore imply that these effects are important well into the thermosphere (altitudes higher than 500 kilometres). This requires both active upper-atmosphere chemistry, consistent with the detection of high-complexity molecules and ions at altitudes greater than 950 kilometres[6,7], and an alternative explanation for the detached haze, such as a transition in haze particle growth from monomers to fractal structures[8].

Saturn's 26.7° obliquity means that Titan's atmosphere experiences large solar flux variations during its 29.5-yr orbit around the Sun. For most of Titan's year, middle-atmosphere (stratosphere and mesosphere at altitudes between 100 and 500 km) circulation is predicted to comprise a single pole-to-pole circulation cell, with summer-hemisphere upwelling, winter-hemisphere subsidence and a winter-hemisphere circumpolar vortex[1,2,5,9–12]. This was confirmed during northern winter using measurements of temperature and trace-gas abundance made by NASA's Cassini spacecraft[13–18]. Titan experienced northern spring equinox on 11 August 2009, around which time changes in solar flux distribution were predicted to cause a reversal of the middle-atmospheric circulation. Such dynamical changes can be probed using profiles of temperature and trace-gas abundance[15] derived from infrared spectra measured with Cassini's Composite Infrared Spectrometer[19] (CIRS). Therefore, to investigate the reversal mechanism we analysed all available south polar limb (horizontal viewing) CIRS observations made in the 4-yr period centred on the equinox. This included measurements at complementary high (0.5 cm^{-1}) and low (14 cm^{-1}) spectral resolutions (Supplementary Information, Supplementary Fig. 1 and Supplementary Table 1).

The CIRS observations show that a very large increase in high-altitude trace-gas emission occurred over the south pole sometime between late 2010 and mid 2011 (Fig. 1). From both high- and low-resolution observation sequences, we derived altitude profiles of temperature, HCN, HC_3N and C_2H_2 using a nonlinear optimal estimation inversion method[20] that closely follows our previous studies[14,21] (Supplementary Information and Supplementary Table 2). Additionally, the high-resolution data allowed determination of C_3H_4, C_4H_2 and C_6H_6 profiles whose emission peaks were too close together to be resolved in the low-resolution data.

Inversion results show very rapid changes in atmospheric temperature and composition, especially after the equinox (Figs 2–4 and Supplementary Fig. 2). The observed south polar warming at altitudes above 300 km suggests that subsidence over the south pole is initiated just after equinox, with the increased temperature being due to adiabatic heating as upper atmosphere air is advected to higher pressures and compressed. This is similar to the process that caused a subsidence-induced north polar hotspot during northern winter[13,22]. The observed temperature structure implies subsidence velocities of 0.5–2.0 mm s^{-1}, broadly consistent with predictions from numerical models (Supplementary Information and Supplementary Table 3). Subsidence is weakest just after equinox in early 2010, at 0.5 mm s^{-1}, but quickly increases to 1.5 mm s^{-1} by June 2010 (2010.43). Cooling observed in the stratosphere (150–300 km) suggests that for the period covered by our data subsidence does not extend to lower altitudes. The cooling by 20 K that is evident between January 2010 (2010.04) and September 2011 (2011.70) at altitudes of 150–300 km (Fig. 4) is most likely due to radiative cooling from the lower atmosphere, which since equinox has been experiencing reduced insolation, and is consistent with the ~1-yr cooling timescale at these altitudes[23].

Changes in upper-atmosphere composition occur on similarly short timescales (Figs 3 and 4 and Supplementary Fig. 2), with evidence of large increases in trace-gas abundances occurring in 2011. This can be explained by a combination of subsidence and photochemically induced vertical gradients. High-altitude (>500 km) photochemical reactions produce trace compounds such as HCN and HC_3N, which are transported into the lower atmosphere by vertical mixing processes, where they are destroyed by photolysis or removed by condensation near the tropopause[24]. The result is increasing relative abundances of these compounds with altitude and a vertical gradient inversely proportional to species lifetime[25]. Subsidence would advect these profiles downwards, causing enrichment at lower atmospheric levels[15] and explaining the observed increase.

Therefore, both observed temperature and abundance increases are consistent with mesospheric (>300 km) south polar subsidence during the post-equinox period. This implies a recent reversal in circulation direction for the south polar mesosphere, relative to the circulation direction derived earlier in the mission[13–16]. An alternative, purely radiative, explanation for the temperature changes can be rejected. Radiative time constants at mesospheric altitudes are short relative to Titan's seasons, and temperature should thus in theory be able to react rapidly to changes in seasonal solar flux. However, photochemical lifetimes of most trace gases are comparable to or greater

[1]School of Earth Sciences, University of Bristol, Wills Memorial Building, Queen's Road, Bristol BS8 1RJ, UK. [2]Atmospheric, Oceanic and Planetary Physics, Department of Physics, University of Oxford, Clarendon Laboratory, Parks Road, Oxford OX1 3PU, UK. [3]Planetary Systems Laboratory, NASA Goddard Space Flight Center, Greenbelt, Maryland 20771, USA. [4]SRON Netherlands Institute for Space Research, Sorbonnelaan 2, 3584 CA Utrecht, The Netherlands. [5]LESIA Observatoire de Paris, CNRS, UPMC Université Paris 06, Université Paris-Diderot, 5 place Jules Janssen, 92195 Meudon Cedex, France. [6]Department of Earth and Space Sciences, University of California Los Angeles, Los Angeles, California 90095-1567, USA.

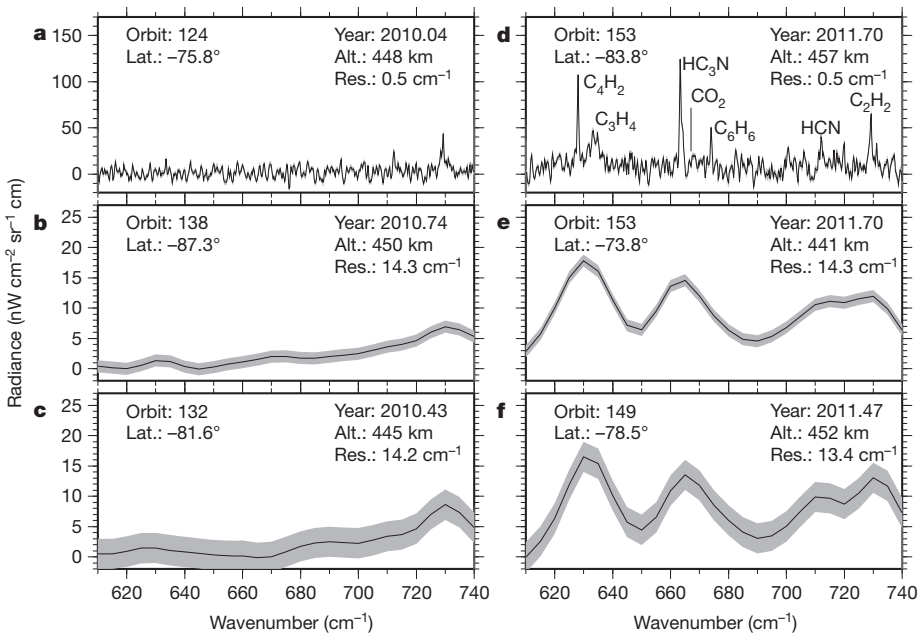

Figure 1 | Rapid south polar atmospheric change observed using infrared spectra. These observations were made using Cassini CIRS after the 11 August 2009 equinox and are grouped as follows: before 1 January 2011 (**a**–**c**); after 1 January 2011 (**d**–**f**). The spectra indicate that between late 2010 and early 2011 there was a large increase in trace-gas emission at the south pole. This is observed in three independent observation sequences at both high and low spectral resolution. Altitude refers to the tangent altitude, which is the closest distance to Titan's surface reached by the line-of-sight vector, and is approximately 450 km for these spectra. Grey areas indicate measurement error envelopes (s.e.). We focused on the 610–740 cm^{-1} (16.4–13.5 μm) spectral region, which contains strong trace-gas emission features. Since the 2009 northern spring equinox, Cassini remained in an equatorial orbit around Saturn, which was ideal for limb sounding (horizontal viewing), and many limb measurements of the south polar region were taken (Supplementary Table 1). Most observations were of a single latitude, but several limb-mapping sequences were also measured, covering multiple latitudes at a time and allowing the determination of latitude–altitude cross-sections through the atmosphere (Figs 2 and 3).

than seasonal timescales. Therefore, to be consistent with all our data, the observed changes must be due to a reversal of the circulation as opposed to changes in direct solar heating.

We note that, whereas the January 2010 (2010.04) temperature results show polar warming at high altitudes almost immediately after equinox, there is no evidence for large increases in trace-gas abundances until much later. In fact, the first evidence for increases in south polar trace gas is in June 2011 (2011.47) (Fig. 3), and this is corroborated by subsequent observations in September 2011 (2011.70) (Fig. 4 and Supplementary Fig. 2). However, unlike increases in south polar temperature caused by adiabatic heating, trace gases take time to advect from upper-atmosphere source regions to observable altitudes, which means that the temporal offset between temperature and composition results is not inconsistent. Our results suggest that this advection process takes approximately 1.5–2 yr after reversal initiation. This corresponds to ~100 km of polar subsidence, assuming the 1.5 mm s^{-1} subsidence rate inferred from polar temperature anomalies.

An independent check on this interpretation and on south polar subsidence rates can be obtained from the composition results themselves. Polar abundance increases at 450 km are at least an order of magnitude for all gases (Fig. 4 and Supplementary Table 4) except C_2H_2, which has a more muted response in keeping with its longer atmospheric lifetime and shallower vertical gradient. A first-order approximation, combining results from all gases and assuming no photochemical alteration of gas profiles, implies average subsidence velocities between January 2010 (2010.04) and September 2011

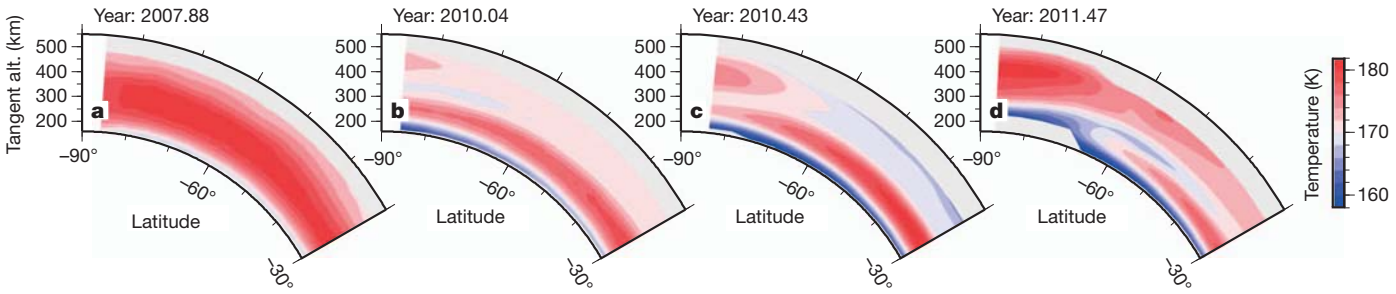

Figure 2 | South polar seasonal temperature changes. Cross-sections were derived from low-spectral-resolution limb-mapping sequences and cover pre-equinox (**a**) and post-equinox (**b**–**d**) periods. Substantial stratospheric (<300 km) cooling occurs after the equinox, consistent with reduced total solar flux during this time[17,23], as Titan moves towards southern winter. After the equinox (after mid-2009), there is evidence for high-altitude (450 km) polar warming relative to more equatorial latitudes. This is initially present as a small (2 K) temperature anomaly almost immediately proceeding the equinox (**b**), which increases to 6 K (**c**) and then to 8 K (**d**) in subsequent sequences. This implies that the mesospheric circulation has reversed and is now subsiding at the south pole. The strongest polar warming occurs in the most recent observation, indicating the fastest subsidence speeds. Grey regions indicate latitudes and altitudes where observations exist but have insufficient signal-to-noise ratios for an accurate temperature determination. Contour spacing is 2 K, which is the maximum uncertainty for this altitude range. These changes are confirmed by additional single-latitude observations at both high (Fig. 4) and low (Supplementary Fig. 2) spectral resolution.

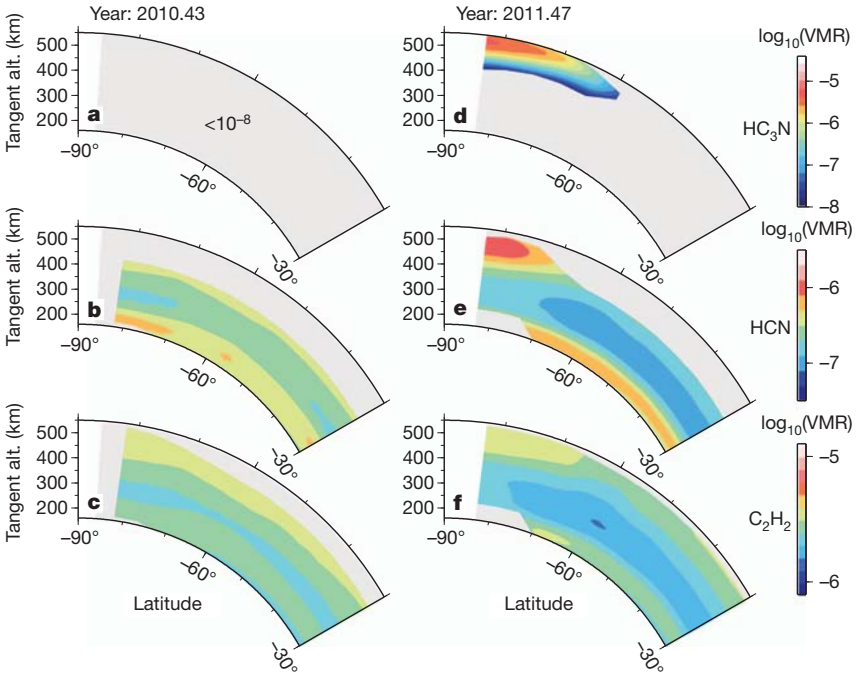

Figure 3 | Seasonal changes in south polar trace-gas abundances. Cross-sections were derived from low-spectral-resolution limb-mapping sequences and show results for June 2010 (2010.43) (**a**–**c**) and June 2011 (2011.47) (**d**–**f**). In the 2011 observation, trace-gas abundances have increased substantially at high altitudes (>450 km) over the south pole. The most pronounced increases occur for HCN and HC_3N. This is consistent with temperature determinations in Fig. 2 and implies a reversal in mesospheric circulation, with subsidence now occurring at the south pole. Grey regions indicate latitudes and altitudes where observations exist but have insufficient signal-to-noise ratios for an accurate abundance determination. We note that HC_3N cannot be reliably determined in June 2010 (2010.43) owing to its very low relative abundance ($<10^{-8}$). Low-resolution mapping sequences taken before June 2010 (2010.43) show comparable compositions to those in **a**–**c**. VMR is the volume mixing ratio and quantifies the relative atmospheric abundance of each species.

(2011.70) of 0.8–2.3 mm s^{-1} (Supplementary Information and Supplementary Table 4). This is in excellent agreement with values of 0.5–2.0 mm s^{-1} derived from the temperature results.

The mechanism for reversal of middle-atmosphere circulation is related to solar flux distribution and angular momentum transfer. Stratospheric temperatures are not symmetric at northern spring equinox, but are slightly warmer in the south[17,23,26]. Therefore, given that temperatures and zonal winds are coupled by the thermal wind equation, during springtime the atmosphere has to transport angular momentum from the pole leaving winter, where the circumpolar

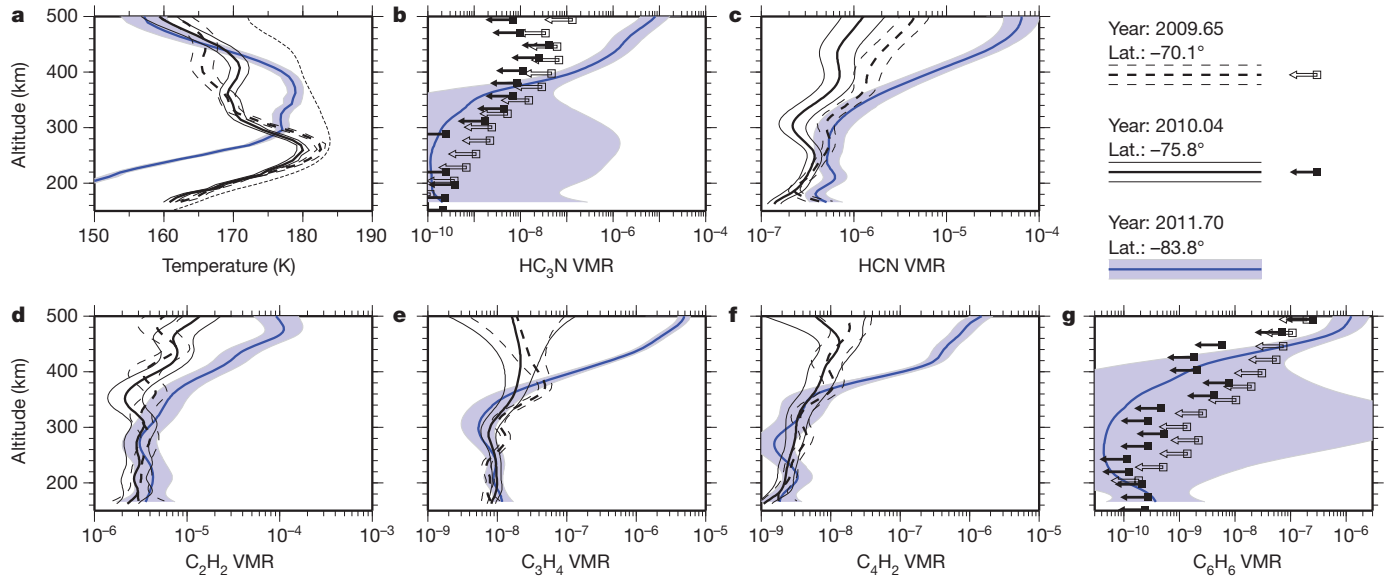

Figure 4 | Profiles of temperature and composition taken close to the equinox. All profiles were derived from high-spectral-resolution (0.5 cm^{-1}), single-latitude limb integrations. **a**, Temperature profiles show evidence for mesospheric polar warming, which increases and moves to lower altitude with time. **b**–**g**, Large increases in all trace-gas species are visible in September 2011 (2011.70). Thin dashed lines, thin solid lines, and light blue shading indicate the error envelope (s.e.) for August 2009 (2009.65), January 2010 (2010.04) and September 2011 (2011.70) observations, respectively. The short-dashed line in **a** indicates the a-priori profile used to start the inversion. HC_3N (**b**) and C_6H_6 (**g**) are not reliably detected in August 2009 (2009.65) or January 2010 (2010.04), so 1σ upper limits are given instead (arrows). These high-spectral-resolution observations confirm the trends seen in the low-spectral-resolution mapping sequences (Figs 2 and 3).

winds are strong, to the pole moving towards winter, where the winds are weak[26]. This results in a cross-equatorial circulation from north to south at high altitudes, driving subsidence in the south polar atmosphere and explaining the observed adiabatic heating and increased trace-gas abundances. Our observations of temperature now constrain the mesospheric reversal timing to shortly after equinox—perhaps coincident with it, but certainly within six months (0.015 Titan years). Furthermore, at present the observed spatial distribution of abundance and temperature increases limits the main zone of subsidence to 90–70° S, with subsidence velocities of 0.5–2.3 mm s^{-1}.

The observed reversal timing agrees very well with recent atmospheric general circulation models[1,2,11]. Unfortunately, direct comparison of observed temperature and composition with results of these models is not possible at the moment because, as noted previously[1,2], the models have a relatively low upper boundary, which means that whereas our peak seasonal signal occurs above 400 km, the models are only applicable at lower altitudes. Decoupling of tropospheric and stratospheric circulation means that this has limited effect on the lowermost atmosphere, and there is generally good agreement between models and observations for the non-superrotating troposphere and the surface[2]. However, the low model top distorts the middle-atmosphere structure and places the polar zonal jets at too low an altitude compared with observational constraints[1,2,23]. Our results show that the reversal in atmospheric circulation takes place throughout the mesosphere, with temperatures implying subsidence in the 300–500-km altitude range and composition implying subsidence up to an altitude of at least 600 km, into photochemical source regions, which is necessary to provide the high trace-gas abundance we observe. Therefore, although the agreement between numerical models and observations is encouraging in terms of reversal timing and approximate reproduction of key atmospheric features such as superrotation and zonal jets, our results show that it is critical for the next generation of models to be extended to higher altitudes to fully capture Titan's dynamical behaviour.

If the circulation does extend to 600 km altitude or more then the detached haze layer observed around 450–500 km cannot mark the top of middle-atmosphere circulation, as has been previously assumed. Recent seasonal changes in the altitude of the detached haze[27] provide a strong argument for circulation-induced modification of the haze, but our observations show that an origin for the detached haze in terms of dynamical transport and a coincident peak haze-production altitude[4] cannot provide a complete explanation. Instead, an origin in a transition from monomer to fractal haze particles[8], combined with higher-altitude haze production and subsequent modification by dynamical circulation, is required. Such high-altitude circulation also needs a driving mechanism, implying that solar heating of haze and cooling due to infrared emission from trace gases is important at higher altitudes than previously thought.

Therefore, a consistent picture of Titan's middle and upper atmospheres is now emerging. Complex chemistry occurs in the uppermost atmosphere, as evidenced by heavy ions and molecules detected by Cassini's *in situ* instruments[6,7,28] and ultraviolet observations of haze opacity in the thermosphere[29], in broad agreement with active thermospheric photochemistry predicted by the most recent one-dimensional photochemical models[24,30]. Our measurements show that the radiative effects of this complex chemistry are sufficient to drive dynamics up to very high altitudes, effectively linking chemical and dynamical processes well into the thermosphere (>500 km).

Received 30 March; accepted 19 September 2012.

1. Newman, C. E., Lee, C., Lian, Y., Richardson, M. I. & Toigo, A. D. Stratospheric superrotation in the TitanWRF model. *Icarus* **213,** 636–654 (2011).
2. Lebonnois, S., Burgalat, J., Rannou, P. & Charnay, B. Titan global climate model: a new 3-dimensional version of the IPSL Titan GCM. *Icarus* **218,** 707–722 (2012).
3. Porco, C. C. *et al.* Imaging of Titan from the Cassini spacecraft. *Nature* **434,** 159–168 (2005).
4. Rannou, P., Hourdin, F. & McKay, C. P. A wind origin for Titan's haze structure. *Nature* **418,** 853–856 (2002).
5. Hourdin, F. *et al.* Numerical simulation of the general circulation of the atmosphere of Titan. *Icarus* **117,** 358–374 (1995).
6. Waite, J. H. *et al.* Ion neutral mass spectrometer results from the first flyby of Titan. *Science* **308,** 982–986 (2005).
7. Coates, A. J. *et al.* Discovery of heavy negative ions in Titan's ionosphere. *Geophys. Res. Lett.* **34,** L22103 (2007).
8. Lavvas, P. P., Yelle, R. V. & Vuitton, V. The detached haze layer in Titan's mesosphere. *Icarus* **201,** 626–633 (2009).
9. Lebonnois, S., Toublanc, D., Hourdin, F. & Rannou, P. Seasonal variations of Titan's atmospheric composition. *Icarus* **152,** 384–406 (2001).
10. Hourdin, F., Lebonnois, S., Luz, D. & Rannou, P. Titan's stratospheric composition driven by condensation and dynamics. *J. Geophys. Res.* **109,** E12005 (2004).
11. Rannou, P., Lebonnois, S., Hourdin, F. & Luz, D. Titan atmosphere database. *Adv. Space Res.* **36,** 2194–2198 (2005).
12. Crespin, A. *et al.* Diagnostics of Titan's stratospheric dynamics using Cassini/CIRS data and the 2-dimensional IPSL circulation model. *Icarus* **197,** 556–571 (2008).
13. Flasar, F. M. *et al.* Titan's atmospheric temperatures, winds, and composition. *Science* **308,** 975–978 (2005).
14. Teanby, N. A. *et al.* Titan's winter polar vortex structure revealed by chemical tracers. *J. Geophys. Res.* **113,** E12003 (2008).
15. Teanby, N. A., Irwin, P. G. J., de Kok, R. & Nixon, C. A. Dynamical implications of seasonal and spatial variations in Titan's stratospheric composition. *Phil. Trans. R. Soc. Lond. A* **367,** 697–711 (2009).
16. Coustenis, A. *et al.* Titan trace gaseous composition from CIRS at the end of the Cassini-Huygens prime mission. *Icarus* **207,** 461–476 (2010).
17. Teanby, N. A., Irwin, P. G. J., de Kok, R. & Nixon, C. A. Seasonal changes in Titan's polar trace gas abundance observed by Cassini. *Astrophys. J.* **724,** L84–L89 (2010).
18. Vinatier, S. *et al.* Analysis of Cassini/CIRS limb spectra of Titan acquired during the nominal mission I. Hydrocarbons, nitriles and CO_2 vertical mixing ratio profiles. *Icarus* **205,** 559–570 (2010).
19. Flasar, F. M. *et al.* Exploring the Saturn system in the thermal infrared: the Composite Infrared Spectrometer. *Space Sci. Rev.* **115,** 169–297 (2004).
20. Irwin, P. *et al.* The NEMESIS planetary atmosphere radiative transfer and retrieval tool. *J. Quant. Spectrosc. Radiat. Transf.* **109,** 1136–1150 (2008).
21. Teanby, N. A. *et al.* Vertical profiles of HCN, HC_3N, and C_2H_2 in Titan's atmosphere derived from Cassini/CIRS data. *Icarus* **186,** 364–384 (2007).
22. Achterberg, R. K., Conrath, B. J., Gierasch, P. J., Flasar, F. M. & Nixon, C. A. Titan's middle-atmospheric temperatures and dynamics observed by the Cassini Composite Infrared Spectrometer. *Icarus* **194,** 263–277 (2008).
23. Achterberg, R. K., Gierasch, P. J., Conrath, B. J., Michael Flasar, F. & Nixon, C. A. Temporal variations of Titan's middle-atmospheric temperatures from 2004 to 2009 observed by Cassini/CIRS. *Icarus* **211,** 686–698 (2011).
24. Lavvas, P. P., Coustenis, A. & Vardavas, I. M. Coupling photochemistry with haze formation in Titan's atmosphere, part II: results and validation with Cassini/Huygens data. *Planet. Space Sci.* **56,** 67–99 (2008).
25. Teanby, N. A., Irwin, P. G. J., de Kok, R. & Nixon, C. A. Mapping Titan's HCN in the far infra-red: implications for photochemistry. *Faraday Discuss.* **147,** 51–64 (2010).
26. Flasar, F. M. & Conrath, B. J. Titan's stratospheric temperatures: a case for dynamical inertia? *Icarus* **85,** 346–354 (1990).
27. West, R. A. *et al.* The evolution of Titan's detached haze layer near equinox in 2009. *Geophys. Res. Lett.* **38,** L06204 (2011).
28. Waite, J. H. *et al.* The process of tholin formation in Titan's upper atmosphere. *Science* **316,** 870–875 (2007).
29. Liang, M.-C., Yung, Y. L. & Shemansky, D. E. Photolytically generated aerosols in the mesosphere and thermosphere of Titan. *Astrophys. J.* **661,** L199–L202 (2007).
30. Krasnopolsky, V. A. A photochemical model of Titan's atmosphere and ionosphere. *Icarus* **201,** 226–256 (2009).

Supplementary Information is available in the online version of the paper.

Acknowledgements This work was funded by the UK Science and Technology Facilities Council, the Leverhulme Trust and the NASA Cassini mission.

Author Contributions N.A.T. designed the study, performed the radiative transfer analysis and wrote the initial manuscript. P.G.J.I., N.A.T., C.A.N., R.d.K. and S.B.C. developed and maintained the radiative transfer code used for the analysis. S.V. performed independent tests on the results. A.C. performed further checks on the inversion method. All authors contributed to the interpretation of the results, in addition to editing and improving the final manuscript.

Author Information Reprints and permissions information is available at www.nature.com/reprints. The authors declare no competing financial interests. Readers are welcome to comment on the online version of the paper. Correspondence and requests for materials should be addressed to N.A.T. (n.teanby@bristol.ac.uk).